applied sciences

MDPI

Article

Estimating the Radioactive Heat Production of a Granitic Rock in the University of A Coruña (Galicia, Northwest Spain) by Gamma-ray Spectrometry

Jorge Sanjurjo-Sánchez [1,*], Victor Barrientos Rodríguez [1], Carlos Arce Chamorro [1] and Carlos Alves [2]

[1] University Institute of Geology, University of A Coruña, Campus de Elviña, 15017 A Coruña, Spain
[2] LandS/Lab2PT-Landscapes, Heritage and Territory Laboratory (FCT-UIDB/04509/2020), Earth Sciences Department, School of Sciences, University of Minho, 4710-057 Braga, Portugal
* Correspondence: jorge.sanjurjo.sanchez@udc.es; Tel.: +34-981167000 (ext. 2695)

Abstract: Geothermal energy is a form of renewable energy with a long tradition in European countries, although it is scarcely used in Spain. One of the reasons for this is the poorly studied geothermal potential of the Spanish territory. In recent years, data published on terrestrial gamma radiation and the geochemistry of radioisotopes in rocks have suggested that the radiogenic heat production (RHP) in some areas of Spain is high. In this work, we assessed the RHP by analysing the U, Th, and K contents of the rocks underlying the most important campus of the University of A Coruña (northwest Spain), using in situ handheld gamma-ray spectrometry (GRS) and X-ray fluorescence spectrometry (XRF). Our results provide a good fit of the radioisotope contents and unexpectedly high RHP, compared with average data observed in similar rocks (granodiorite). These results reveal that GRS is a very reliable tool for studying the RHP of rock surfaces, and that geothermal energy can be used in the area (i.e., the studied campus, but also most of the city of A Coruña, as it is built on the same underlying rock) for central heating in buildings using ground-source heat pumps (GSHPs).

Keywords: geothermal energy; radiogenic heat production; radioisotope content; gamma-ray spectrometry; granitoid

Citation: Sanjurjo-Sánchez, J.; Barrientos Rodríguez, V.; Arce Chamorro, C.; Alves, C. Estimating the Radioactive Heat Production of a Granitic Rock in the University of A Coruña (Galicia, Northwest Spain) by Gamma-ray Spectrometry. *Appl. Sci.* **2022**, *12*, 11965. https://doi.org/10.3390/app122311965

Academic Editors: David Bertermann, Jin Luo and Joachim Rohn

Received: 5 November 2022
Accepted: 20 November 2022
Published: 23 November 2022

1. Introduction

Although the term geothermal energy can be employed to describe the internal energy of the Earth, in terms of its use as a source of energy it refers to the thermal energy stored in the Earth's crust. The main sources of this geothermal energy are the residual energy available from planet formation and the energy continuously generated from primordial radionuclide decay [1,2]. In practice, geothermal resources consist of thermal energy stored in both rock and trapped steam or liquid water. Such sources provide energy with two possible uses: electricity generation, and direct heat use. The former can be achieved under a steep geothermal gradient when high temperatures are observed in some areas of the Earth's upper crust. The latter is attainable even when the heat stored is considered to be low, which occurs in most of the Earth's crust due to the relatively low thermal conductivity of rocks [3]. This second type of geothermal energy can be harnessed with low-enthalpy technologies such as ground-source heat pump (GSHP) and groundwater heat pump (GWHP) systems [4].

Geothermal energy is counted among renewable energies, with a long tradition, experience, and great potential for the future [5]. A directive by the European Parliament and the European Council established that this type of energy should be considered renewable in countries of the European Union [6]. Despite this directive, the development and use of such energy is poor in countries such as Spain when compared with other countries of the EU, as well as when considering the estimates of potential geothermal energy in this country [7–9]. Although its potential development depends on the energy

policy, a good assessment of the geothermal potential is essential to provide present and future projections of its potential use. In this work, we focus on a local case study in northwest Spain in an attempt to reflect the high potential of this energy in some areas of the country and the need for establishing both development and investment plans for its exploration.

Even though the European Geothermal Energy Council [10] has stated that its objectives until the year 2050 include the establishment of a European geothermal industry base (2020) or obtaining a substantial part of the electricity supply from geothermal energy (2050), these objectives are far from being fulfilled in Spain. Studies of geothermal potential carried out in Spain in the last 45 years have been few and have often been reduced to conservative estimates obtained from theoretical or tabulated parameters [7,11]. In most of the territory of Spain, based on the VDI 4640 (2001) standard [12], it has been estimated that there is a very low heat flux, with medium enthalpy resources (temperatures between 100 °C and 150 °C) and very low enthalpy (T < 30 °C), with some exceptions—such as the Canary Islands [7]. This standard establishes estimated values to assess the geothermal potential, without considering how the variability in the mineral composition of rocks affects their thermal conductivity and, above all, the variable heat generation in them due to their contents of primordial radioisotopes of uranium, thorium, and potassium. The most ambitious study carried out by the Institute for the Diversification and Saving of Energy [7] acknowledges, in fact, that its own estimates are conservative. Currently, there are more precise studies to estimate the real geothermal potential, although with poor spatial resolution [8]. For the northwest of Spain, it has been proposed that the geological characteristics may be of particular interest for the use of geothermal energy through GSHPs [13].

In recent years, published studies have provided data on terrestrial gamma radiation [14], potential radon emissions [15], and even data on the geochemical composition of radioisotopes on the surface, in the first Geochemical Atlas of Spain [16]. These new data, separately, have made it possible to observe that in northwest Spain, both U and Th isotopes are especially abundant in certain rocks (such as granites), exceeding the average values for this type of rock [17–19]. These radioisotopes are responsible for 85% of the heat production in rocks by radioisotopes [17], so they are the main cause of the geothermal gradient at the surface of the crust being higher than the average gradient. Due to this abundance of U and Th, very high values of terrestrial gamma radiation and potential emission of radon in rocks are observed in the autonomous community of Galicia [14,15]. In this region, granitic rocks originating during the Variscan Orogeny are especially abundant, in which high concentrations of U, Th, and K have been observed [13,20], exceeding the average concentrations expected in granites, as occurs in some Palaeozoic granites [17–19]. Despite this, the geothermal potential of this area has not yet been studied in detail.

1.1. Radiogenic Heat Production

Rocks contain variable amounts of primordial radionuclides that generate heat to a certain extent, due to the conversion of the radioactive decay mass to energy. These include ^{40}K and the radioisotopes of the decay series of ^{238}U, ^{235}U, and ^{232}Th.

The heat generated by the natural radioactive decay in the Earth's crust constitutes a substantial portion of the terrestrial heat flow. Some authors [21,22] have proposed that the radiogenic heat production of granite rocks (RHP in $\mu W \cdot m^{-3}$) can be calculated by taking into account the heat generation constant (i.e., the amount of heat released per unit time and per gram of U, Th, and K) and the uranium, thorium, and potassium concentrations (C_U, C_{Th}, and C_K, respectively) in a rock by using the following expression:

$$\mathrm{RHP} = 10 - 5\,\rho\,(9.52\,C_U + 2.56\,C_{Th} + 3.48\,C_K) \quad (1)$$

where ρ is the density of the rock (kg m^{-3}) and C_U, C_{Th}, and C_K are the concentrations of uranium (weight ppm), thorium (weight ppm), and potassium (weight %), respectively.

The heat production unit (μWm^{-3}) may be converted into heat generation units (1 HGU = 10^{-13} cal cm^{-3} s^{-1}) by the equivalence 1 HGU = μW m^{-3} estimated for the Gansboden granite gneiss at the Guspisbach heat flow site in the Central Alps of Switzerland [23]. The radioelement concentration (Ur) is calculated by Ur equivalents: 1 ppm of U in equilibrium (1 ppm eU) = 1 Ur; 1 ppm of Th equilibrium (1 ppm eTh) = 0.5 Ur; 1 wt % of K = 2 Ur [24,25].

The RHP is a scalar petrophysical property independent of in situ temperature and pressure. Both ^{232}Th and ^{238}U are the most important radionuclides that contribute to heat production (about 85%), while ^{40}K contributes to a lesser extent [17]. They also give rise to daughter radionuclides present in the Earth's crust rocks, with the U and Th decay chains being the most geologically significant in such heat production.

There are several methods that allow determination of the radioisotope concentrations in rocks for assessing the rate of heat production. Some laboratory analytical techniques indirectly assess the activity concentrations in rock samples, namely, inductively coupled plasma atomic emission spectrometry and mass spectrometry, instrumental neutron activation analyses, and X-ray fluorescence spectrometry. Low background gamma-ray spectrometry directly estimates the activity concentrations of such radionuclides [22,26]. The latter technique is the only one that gives direct indication of any possible disequilibrium in the U and Th decay chains. However, disequilibrium is infrequent in rocks [27].

It is also possible to assess the concentrations of radioisotopes by handheld, carborne, and airborne gamma-ray spectrometry. These techniques are used for estimating the concentrations of radioelements in the surface rocks, and borehole gamma-ray spectrometry is used to acquire a continuous spectrum of the U, Th, and K concentrations of subsurface rocks [28]. This kind of field method allows a quick, albeit imprecise, assessment of the radioisotope contents of rocks, making it possible to assess the heat production from these data [29]. Laboratory analyses require fieldwork, sampling, and analyses that are costly and time-consuming. However, portable gamma-ray spectrometry (GRS) can be a quick and cheap procedure. When GRS measurements are carried on rock outcrops, a $2\pi r$ geometry (plain area) is needed to avoid over- or underestimation of the radioisotopes of K, U, and Th [29].

1.2. Aim of the Study

In this work, our main goal was to assess the potential radiogenic heat production of the underground rock underlying the main campus of the University of A Coruña (A Coruña, northwest Spain). To that end, we analysed the K, Th, and U contents of rock outcrops on the campus. We also estimated the K, Th, and U contents of the sampled rock outcrops by GRS, for comparison purposes. We built radionuclide and heat production maps of the campus based on these data, to confirm whether GRS is suitable for estimation of the RHP, with the prospect of being used in the future for the use of geothermal energy on the campus and exploring the RHP of the area with GRS.

2. Study Area

The autonomous community of Galicia (northwest Spain) is mostly on Precambrian and Palaeozoic basic–ultrabasic metamorphic and granitoid rocks [20]. Three types of granitic rocks can be found: calc-alkaline syncinematic, peraluminous syncinematic and late-collisional cinematic, and calc-alkaline late-collisional [20]. In the first group, both granodiorite and monzogranites are the most frequent, with high values of K [30]. Peraluminous granitoids—the most abundant—vary widely in composition and texture [31], while a range of monzogranites predominate among late-collisional granites [32]. One of the most extended peraluminous granitoid is the granodiorite of A Coruña. The rock is present in most of the area of the city of A Coruña (about 80%), which has 250,000 inhabitants (Figure 1), with around 90% of the population (around 225,000) living in the area of such rock.

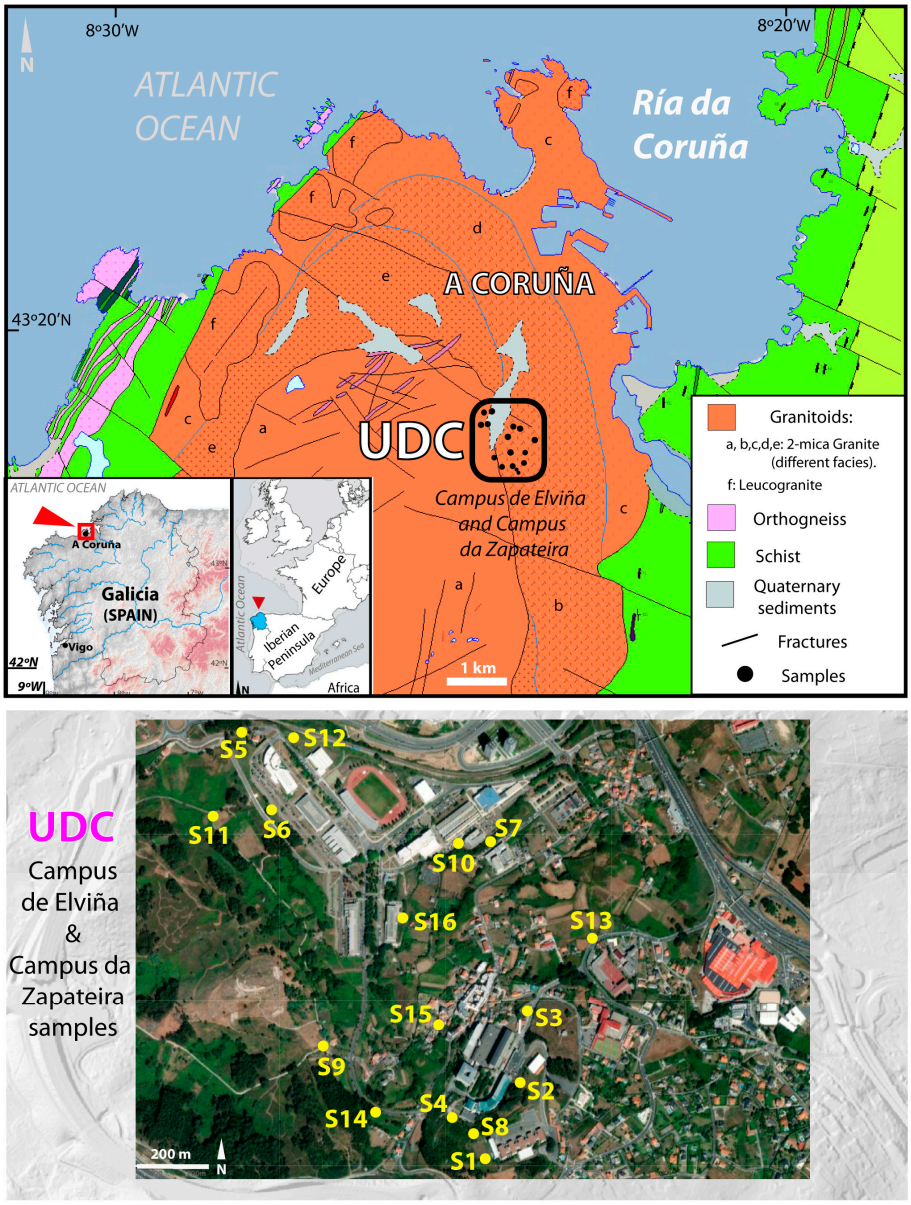

Figure 1. Location of the Elviña-A Zapateira campus of the University of A Coruña (northwest Spain), with a geological map of the study area (modified from [33]). Satellite image from Google Earth. Sampling sites are marked and explained in Table 1.

The main campus of the University of A Coruña (Elviña-A Zapateira) is located on this rock. Such rock shows two facies: early-stage and late-stage; both are very similar in colour (grey), texture (coarse-grained), and chemical and mineralogical composition, with quartz, plagioclase, microcline, and biotite as the main minerals [20]. More muscovite is observed in the late stage. The rock is usually weathered, showing an ochre colour and loss of cohesion. According to the geological map of the city (and campus) of A Coruña, the contact between both facies is located in the Elviña campus area, although at present it is below the buildings and urban structures of the campus and below the sediments in some parts. In this study, we sampled both facies.

Table 1. Position and coordinates of the studied outcrops and samples (WGS84). WD: weathering degree.

Sample	Latitude	Longitude	WD	Location
P1	43°19′31.19″ S	8°24′31.6″ W	I	Back of the Professors′ building in Faculty of Philology
P2	43°19′37.78″ S	8°24′27.48″ W	I	Slope between Faculties of Philology and Sciences
P3	43°19′43.98″ S	8°24′26.4″ W	I	Beside Casa del Francés
P4	43°19′34.81″ S	8°24′35.39″ W	I	Beside Faculty of Sciences
P5	43°20′8.71″ S	8°25′0.23″ W	I	Beside UDC kindergarten
P6	43°20′1.72″ S	8°24′56.7″ W	I	Car park of Faculties of Law and Education
P7	43°19′58.71″ S	8°24′30.59″ W	II	Back of CICA building
P8	43°19′33.25″ S	8°24′33.09″ W	II	Southwest of Faculty of Sciences
P9	43°19′41.17″ S	8°24′50.83″ W	II	Surroundings of Castro de Elviña archaeological site
P10	43°19′58.71″ S	8°24′34.59″ W	III	Car park of the Schools of Civil Engineering and Informatics
P11	43°20′1.23″ S	8°25′3.59″ W	II	Path in front of Faculty of Law
P12	43°20′7.99″ S	8°24′54.14″ W	II	Close to Sports Centre
P13	43°19′50.19″ S	8°24′19.05″ W	I	Monument to Elviña's Battle
P14	43°19′35.55″ S	8°24′44.64″ W	III	Slope intercampus road
P15	43°19′42.9″ S	8°24′37.05″ W	III	Canedo 15, Elviña
P16	43°19′52.23″ S	8°24′41.22″ W	V	Slope Central Research Service

The Elviña-A Zapateira campus (Figure 1) has a total surface area of 63 ha and 27.3 ha of built area distributed over 20 buildings: 12 for teaching and 8 for sports, research, and administrative use. Most of these buildings were built between 1995 and 2006 and are used for 13–14 h a day. The vast majority are heated by gas oil, except for five that are heated by electric radiators and one with a heat pump [34]. The total average annual consumption for these buildings is approximately 14,300 MWh [34]. The average annual consumption of diesel for heating is 9500 MWh/year, which is equivalent to approximately 725,880 litres of diesel. This fuel generates CO_2 emissions of 260 tons per year on average.

3. Materials and Methods

3.1. Sampling and Data Acquisition

Selection of locations on the campus for sampling was performed after a preliminary exploration was carried out via Google Earth and considering the geological map. As the contact between the two granodiorite facies occurs in the campus area (the early-stage facies on the west and the late-stage facies on the east of the campus), we considered both facies in the sampling process. After the preselection of areas of interest, a walking field exploration was carried out, looking for rock outcrops. Most such outcrops were located in the west and south parts of the area. A total of 16 outcrops of both facies were chosen for the study (Table 1 and Figure 1). In such outcrops, gamma-ray spectrometry measurements were performed, and rock samples were taken for geochemical analyses on the same outcrops where the gamma-ray measurements were carried out.

3.2. In Situ Gamma-Ray Spectrometry

Gamma-ray spectra were acquired in situ in the field with a portable gamma-ray spectrometer (GF Instruments Gamma Surveyor Vario), equipped with a BGO probe ($Bi_4Ge_3O_{12}$) with 2018 channels, along with a 51 mm × 51 mm detector (103 cm^3) with probe dimensions of 70 mm and a length of 290 mm (VB6), and a shielded photomultiplier. This equipment enables measurement of energies up to 3 MeV. Measurements were taken by direct probe contact at rock outcrops with variable geometry. We followed the recommendations given by the International Atomic Energy Agency (IAEA), as described by Erdi-Krausz et al. [28] for static measurements (i.e., recording a spectrum in a given point during a specific amount of time). A period of 180 s is recommended by the manufacturer to optimise time and precision. Statistical error uncertainties—estimated to be 6% for K, 30% for U, and 16% for Th—were considered, according to the manufacturer's specifications for low gamma-ray emissions. http://www.gfinstruments.cz/index.php?

menu=gi&smenu=igr&cont=surveyor_V_&ear=ts (accessed on 11 October 2022). These errors were due to background radiation that mostly originated from three main sources: atmospheric radon and its daughters, cosmic rays, and instrument background radiation. Moreover, the geometry of measured surface must be planar ($2\pi r$ geometry), as possible surface roughness of the measured terrain and any nearby topographic features can both cause possible inaccuracies in the measurements. A second measurement was carried out for each studied outcrop using a lead collimator specially designed by the device's manufacturer to reduce the background gamma radiation from surroundings.

From these spectra, we can extract estimated contents of K (potassium, mass percentage), eU (uranium equivalents, in mass parts per million (ppm)), and eTh (thorium equivalents, also in ppm). While potassium contents were estimated from the peak of ^{40}K at 1.461 MeV (energy range 1.366 keV–1.564 keV), there were several radioactive isotopes in the uranium and thorium decay series. Thus, we used "equivalents" of uranium and thorium, assuming secular equilibrium. Estimations of eU and eTh were made from peaks of ^{214}Bi (bismuth) at the 1.764 MeV peak (energy range 1.57 keV–1.959 keV) and ^{208}Tl (thallium) at the 2.615 MeV peak (energy range 2.42 keV–2.81 keV), respectively.

3.3. Geochemical Analyses

For comparison with data acquired with the gamma-ray spectrometer, the rock samples were analysed via X-ray fluorescence spectrometry (XRF) to assess the contents of both major and minor elements in the rock samples. The samples were crushed to a grain size below 63 µm, and XRF measurements were performed using a Bruker-Nonius S4 Pioneer wavelength-dispersive fluorescence spectrometer under helium purging at the University of A Coruña.

To assess trace elements, inductively coupled plasma mass spectrometry (ICP-MS) was used. ICP-MS analyses were carried out using a Thermo Scientific™ ELEMENT XR™ ICP-MS device. For sample preparation, the powdered samples were mixed with an equal amount of lithium tetraborate flux, placed in a carbon crucible, and fused at 1000 °C in a furnace for 30 min. After cooling off the melt, the resultant fusion bead was briefly ground and dissolved in 100 mL of 4% HNO_3/2% HCl_3 solution, which was then analysed by ICP-MS.

The density of the samples was estimated using an Accupyc 1340 Micromeritics gas pycnometer, which used 99.995% pure helium to determine the real density of samples, by measuring the pressure change of helium in a calibrated volume.

3.4. Geographic Information System

Spatial data processing was carried out using the QGIS geographic information system (v.2.18.25). Using this software, an interpolation of the data was carried out for geochemical analyses and GRS data, using the inverse distance weighting (IDW) method of the values obtained for the concentrations of U, Th, and K, as well as the values obtained for RHP. Both types of data were projected onto the MDT05-LiDAR digital terrain models corresponding to sheets H0021 and H0045 [35], based on the UTM coordinates of each sampling point.

4. Results

4.1. Geochemical Analyses

The XRF results (Table 2) indicated that the samples' results were in the usual range between granodiorites and granites sensu stricto [36], since half of the samples had a higher SiO_2 content than expected for granodiorites. The SiO_2 contents ranged between 74.36% (P7) and 62.9% (P15), with an average of 69.04%, although in one sample it was 53.7% (P16). This Si enrichment was observed in both facies and seemed more common towards the south of the study area. Similarly, the concentrations of Al_2O_3 ranged between a maximum of 17.1% (P12) and a minimum of 13.12% (P2), being even higher in sample P16 (21.1%), with an average of 15.53%. In sample P16, the concentration of Fe_2O_3 was atypically high, while that of Na_2O was atypically low. This was due to its high weathering, making it a

saprolite (i.e., grade V in the weathering classifications, [37]). The remainder of the samples were between grades I and III of weathering. Given the importance of K_2O in the calculation of the rate of heat potential, the concentration of K (%) was estimated stoichiometrically from these data (Table 3). This enabled comparison of the K concentration estimated by XRF with that estimated by GRS.

Table 2. Oxides provided by XRF results (in %) and estimated density (in kg m^{-3}).

Sample	SiO_2	Al_2O_3	Fe_2O_3	CaO	MgO	Na_2O	K_2O	TiO_2	MnO	P_2O_5	SrO	BaO	ZrO_2	LOI	Total	Density (kg m^{-3})
P1	70.04	14.96	2.66	1.12	0.45	3.32	4.54	0.21	0.05	0.07	0.03	0.06	<0.001	2.35	99.88	2.646
P2	71.4	13.12	3.64	1.59	0.85	2.9	3.8	0.36	0.07	0.22	0.03	0.07	<0.001	1.84	99.9	2.663
P3	69.88	14.15	3.03	1.32	0.81	2.76	5.16	0.35	0.06	0.17	0.03	0.09	<0.001	2.1	99.91	2.644
P4	72.73	13.96	1.99	0.36	0.39	2.81	4.34	0.25	0.02	0.08	0.01	0.04	<0.001	2.93	99.92	2.656
P5	71.57	14.46	2.12	0.94	0.47	3.26	4.88	0.24	0.03	0.23	0.02	0.05	<0.001	1.66	99.93	2.656
P6	72.42	14.62	1.36	0.52	0.37	2.8	5.1	0.23	0.02	0.18	0.02	0.05	<0.001	2.24	99.93	2.666
P7	74.36	14.37	1.22	0.2	0.15	3.26	4.28	0.05	0.03	0.08	0.01	0.02	<0.001	1.93	99.96	2.674
P8	71.1	14.86	2.21	0.37	0.38	3.23	5.2	0.23	0.03	0.09	0.01	0.05	<0.001	2.16	99.92	2.65
P9	71.67	14.32	2.18	0.45	0.49	2.36	5.14	0.26	0.02	0.17	0.02	0.05	<0.001	2.78	99.91	2.638
P10	67.29	15.7	3.3	1.69	0.85	3.59	5.34	0.35	0.08	0.17	0.05	0.09	<0.001	1.42	99.92	2.679
P11	68.7	16.3	1.2	1	0.44	4.9	5.4	0.19	0.024	0.22	0.009	<0.008	0.013	1.5	99.948	2.656
P12	67.4	17.1	1.4	0.81	0.68	4.1	6.1	0.24	0.019	0.29	0.011	<0.008	0.015	1.8	100.025	2.654
P13	72.3	13.2	2.4	1.6	0.99	3.7	4.1	0.35	0.053	0.22	0.026	0.052	0.026	0.9	99.957	2.688
P14	67.2	17.1	1.4	0.75	0.47	4.8	5.3	0.23	0.027	0.25	0.015	<0.008	0.014	1.9	99.575	2.672
P15	62.9	19.1	1.7	1.3	0.56	4.4	7.4	0.22	0.039	0.1	0.032	0.12	0.018	1.8	99.777	2.635
P16	53.7	21.1	8.1	0.43	1.3	1.2	5.2	0.71	0.032	<0.005	0.014	0.05	0.071	7.6	99.578	2.619
Mean	69.04	15.53	2.49	0.90	0.60	3.34	5.08	0.28	0.04	0.17	0.02	0.06	-	2.31	99.88	2.66
Sd	4.97	2.17	1.67	0.49	0.29	0.94	0.85	0.14	0.02	0.07	0.01	0.03	-	1.50	0.13	0.02

Table 3. Results of GRS measurements and geochemical analyses.

Scheme	GRS			GRS with Collimator			XRF + ICPMS		
	U (ppm)	Th (ppm)	K (%)	U (ppm)	Th (ppm)	K (%)	U (ppm)	Th (ppm)	K (%)
P1	16.7	46.6	4.63	20.3	45.4	4.38	24.9	36.5	3.77
P2	12.2	44.9	4.24	14.7	45.4	4.26	20.7	52.1	3.15
P3	18.9	45.4	4.27	22.5	43.6	4.17	15	42.4	4.28
P4	7.2	17.6	4.65	9.4	17.1	4.38	16.25	25.5	3.60
P5	10.3	19.8	4.23	13	18.3	3.95	12.15	24.4	4.05
P6	11.9	24.3	4.7	16.3	22.1	4.28	16.5	22.9	4.23
P7	14.8	50.5	5.16	17.4	53.7	5.16	2.35	4.68	3.55
P8	11.5	23.2	4.52	14.2	21.8	4.26	12.35	22	4.32
P9	9.8	25.4	5.08	11.3	24.5	5.43	14.4	26.4	4.27
P10	14.5	46.4	4.48	17.9	48.7	4.05	10.35	61.2	4.43
P11	9.1	20.7	4.78	11.9	23.3	4.72	9.83	19.15	3.23
P12	8.5	23.2	4.21	11.1	23.6	3.65	17.5	21.7	3.64
P13	11.5	57.1	6.23	13.4	54.1	6.4	14.45	49.6	2.45
P14	18.2	31.9	6.77	23	30	6.68	22	23.2	3.17
P15	33.8	106.8	12.76	9.9	26.7	2.54	15	33.6	4.42
P16	17.1	60.2	6.71	23	67.3	6.35	24	73.1	3.11
Mean	14.13	40.25	5.46	15.48	33.65	3.73	15.58	35.35	4.67
Sd	6.34	22.78	2.12	5.72	17.80	0.59	4.66	15.59	1.10

The density measurements (Table 2) show that it ranged between 2.619 kg m^{-3} and 2.688 kg m^{-3}, with an average value of 2.660 kg m^{-3}. The lowest value corresponded to the more weathered sample (P16).

The ICP-MS results provide the concentrations of U (ppm) and Th (ppm) in the samples studied. Table 3 shows these data and includes an estimate of the K concentration obtained by XRF, which was used to estimate the geothermal potential. The values obtained for U ranged between 2.45 ppm and 24.9 ppm, with an average of 15.6 ppm. The lowest value, observed in sample P7, was atypical when compared to the rest of the samples, since the closest was 9.83 ppm (P11). These data allow us to compare the concentration of U

with that of Th through the Th/U ratio (Table 4). In the samples studied, the ratio ranged between 0.25 and 0.74 from the geochemical analyses (Table 4), with the average Th/U ratio being 0.49. In the case of K, the range was smaller—between 2.45% and 4.43%, with the average being 4.67%, and without outliers (Table 3).

Table 4. Estimated ratios of Th/U and K/U for the geochemical analyses and GRS measurements. U, Th, and K ratios obtained by geochemical analyses and the two different GRS measurements are also provided. Outliers are marked in red.

Sample	GRS		GRS with Collimator		XRF + ICP-MS		GRS/GRS with Collimator			GRS/XRF + ICP-MS			GRS with Collimator/XRF + ICP-MS		
	Th/U	K/U	Th/U	K/U	Th/U	K/U	U/U	Th/Th	K/K	U/U	Th/Th	K/K	U/U	Th/Th	K/K
P1	0.68	3.61	0.36	4.63	0.45	6.61	0.82	1.03	1.24	0.67	1.28	1.23	0.82	1.24	1.16
P2	0.40	2.88	0.27	3.45	0.32	6.56	0.83	0.99	0.87	0.59	0.86	1.34	0.71	0.87	1.35
P3	0.35	4.43	0.42	5.40	0.52	3.50	0.84	1.04	1.03	1.26	1.07	1.00	1.50	1.03	0.97
P4	0.64	1.55	0.41	2.15	0.55	4.51	0.77	1.03	0.67	0.44	0.69	1.29	0.58	0.67	1.22
P5	0.50	2.43	0.52	3.29	0.71	3.00	0.79	1.08	0.75	0.85	0.81	1.04	1.07	0.75	0.98
P6	0.72	2.53	0.49	3.81	0.74	3.90	0.73	1.10	0.97	0.72	1.06	1.11	0.99	0.97	1.01
P7	0.50	2.87	0.29	3.37	0.32	0.66	0.85	0.94	11.47	6.30	10.79	1.45	7.40	11.47	1.45
P8	0.56	2.54	0.50	3.33	0.65	2.86	0.81	1.06	0.99	0.93	1.05	1.05	1.15	0.99	0.99
P9	0.55	1.93	0.39	2.08	0.46	3.38	0.87	1.04	0.93	0.68	0.96	1.19	0.78	0.93	1.27
P10	0.17	3.24	0.31	4.42	0.37	2.34	0.81	0.95	0.80	1.40	0.76	1.01	1.73	0.80	0.91
P11	0.51	1.90	0.44	2.52	0.51	3.05	0.76	0.89	1.22	0.93	1.08	1.48	1.21	1.22	1.46
P12	0.81	2.02	0.37	3.04	0.47	4.80	0.77	0.98	1.09	0.49	1.07	1.16	0.63	1.09	1.00
P13	0.29	1.85	0.20	2.09	0.25	5.90	0.86	1.06	1.09	0.80	1.15	2.54	0.93	1.09	2.61
P14	0.95	2.69	0.57	3.44	0.77	6.95	0.79	1.06	1.29	0.83	1.38	2.14	1.05	1.29	2.11
P15	0.45	2.65	0.32	3.90	0.37	3.39	3.41	4.00	3.18	2.25	3.18	2.89	3.41	3.18	2.89
P16	0.33	2.55	0.28	3.62	0.34	7.72	0.74	0.89	0.92	0.71	0.82	2.16	0.96	0.92	2.04
Mean	0.53	2.60	0.38	3.41	0.49	4.56	0.80	1.01	1.04	0.81	1.00	1.41	1.01	0.99	1.37
Sd	0.20	0.73	0.10	0.93	0.16	1.75	0.04	0.07	0.06	0.27	0.20	0.48	0.32	0.19	0.50
R	0.88	0.85	0.62	0.47	0.48	−0.38	0.98	0.99	0.97	0.50	0.90	−0.62	0.54	0.93	−0.64

The GRS allowed us to estimate the concentrations of U, Th, and K in the outcrops studied and from which the samples analysed in the laboratory were taken. The results of the measurements taken by the GRS, with and without the collimator, are shown in Table 3 and Figure 2. These data can be compared with those of K concentration obtained by XRF and those of U and Th concentrations obtained by ICP-MS. Comparatively, the estimates of the concentration of U by the GRS with and without a collimator were similar (Figure 2A), with a slight average overestimation of 20% being observed in the measurements made with the collimator (Tables 3 and 4), although one of the samples (P15) provided a very considerable underestimation, which is why it was excluded from the comparison. For Th, the collimator measurements provided a very good fit, with a ratio of 1.01 (Figure 2D and Tables 3 and 4). A relationship similar to that of Th was obtained for K, with a ratio of 1.04 (Figure 2G and Tables 3 and 4).

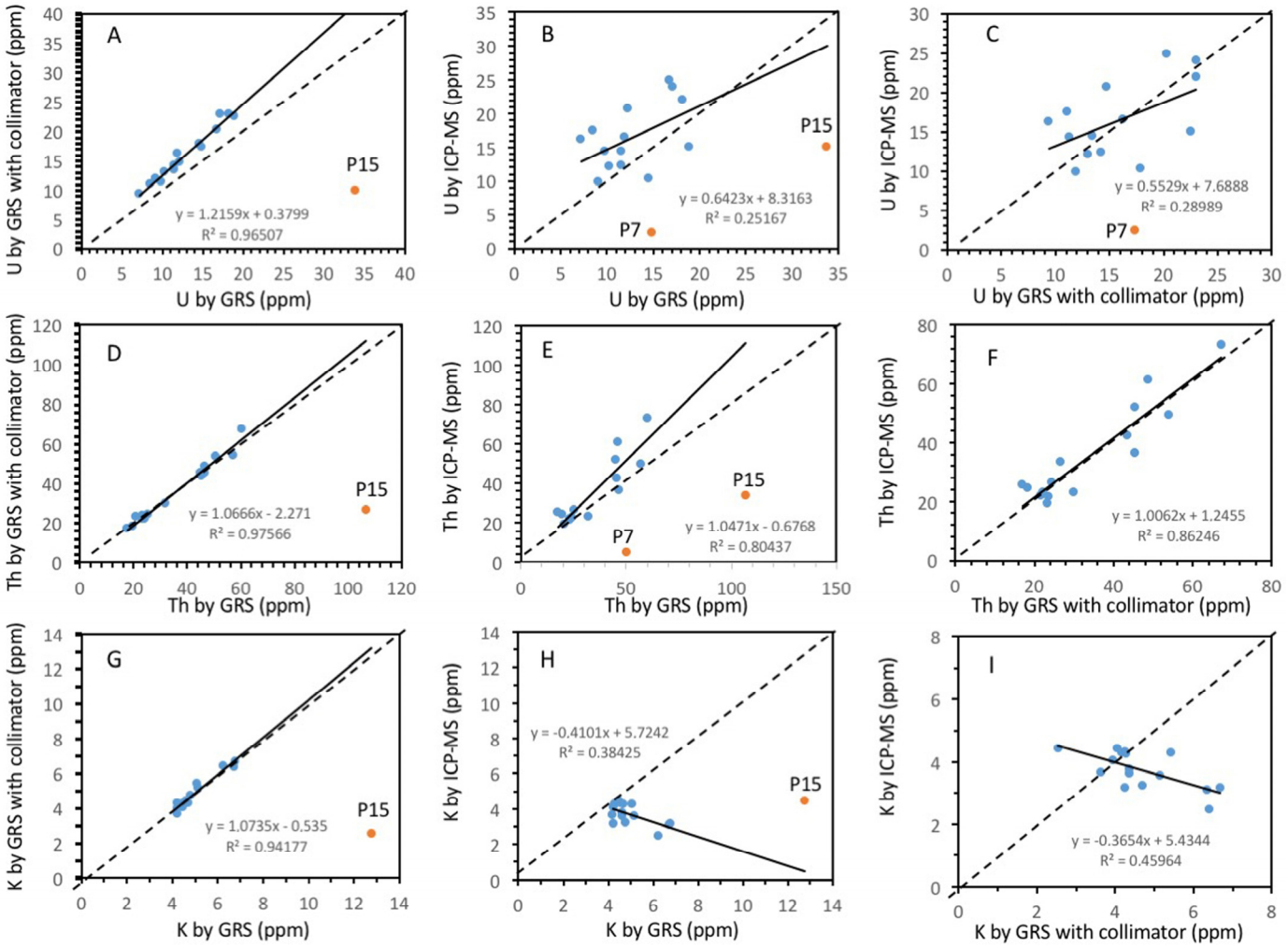

Figure 2. Estimated contents of the different studied elements with geochemical analyses and GRS: (**A**,**D**,**G**) estimated contents obtained by GRS without vs. with collimator; (**B**,**E**,**H**) estimated contents obtained by GRS without collimator vs. geochemical analyses (XRF + ICP-MS); (**C**,**F**,**I**) estimated contents obtained by GRS with collimator vs. geochemical analyses (XRF + ICP-MS).

Comparing the estimates of U obtained by GRS and ICP-MS, it can be seen that the measurements made with and without the collimator underestimate the concentrations obtained via ICP-MS by 20% (ratio = 0.81) (Figure 2B,C and Tables 3 and 4) if we exclude the abnormally low differences in samples P7 and P15 (including these two samples, it is overestimated by 50%). In the case of Th (Figure 2E,F and Tables 3 and 4), samples P7 and P15 also provide atypical differences for measurements with and without the collimator, and the ratio of both without considering these samples is close to 1.00 (without the collimator) and 0.99 (with the collimator). For K, greater variability is observed in the results (Figure 2H,I and Tables 3 and 4), and the average ratio between the measurements with the collimator and XRF is 1.37, while the average ratio without the collimator is very similar (1.41), without considering the sample P15. Therefore, GRS overestimates the K concentration by approximately 40%. In fact, a negative correlation can be observed between the K estimates made by GRS and the geochemical analyses (Figure 2H,I and Table 4).

4.2. Geothermal Potential

For the whole set of samples, the results of calculating the radiogenic heat production (RHP) indicate a value of 6.54 ± 2.25 μW m^{-3} (Table 5). Sample P7 is the one with the lowest RHP (1.20 μW m^{-3}), being is clearly different from the other samples. The range of

results oscillates between this value and the maximum, provided by samples P1 and P2 (both 9.10 μW m^{-3}).

Table 5. Radiogenic heat potential (RHP) and ratios of RHP estimates obtained via the different methods.

Sample	Estimated HGP			Ratio of Estimated HGPs		
	GRS	GRS Collimator	XRF + ICP-MS	GRS/GRS Collimator	GRS/XFR + ICPMS	GRS Collimator/FRX + ICPMS
P1	7.78	8.60	9.13	0.90	0.85	0.94
P2	6.53	7.21	9.13	0.91	0.72	0.79
P3	8.23	9.02	7.03	0.91	1.17	1.28
P4	3.40	3.91	6.18	0.87	0.55	0.63
P5	4.32	4.89	5.09	0.88	0.85	0.96
P6	5.09	6.04	6.14	0.84	0.83	0.98
P7	7.68	8.57	1.20	0.90	6.39	7.13
P8	4.87	5.44	4.99	0.89	0.98	1.09
P9	4.60	4.95	5.78	0.93	0.80	0.86
P10	7.29	8.29	7.22	0.88	1.01	1.15
P11	4.11	5.00	4.07	0.82	1.01	1.23
P12	4.08	4.73	6.25	0.86	0.65	0.76
P13	7.40	7.70	7.36	0.96	1.01	1.05
P14	7.41	8.51	7.52	0.87	0.99	1.13
P15	16.79	4.52	6.43	3.72	2.61	0.70
P16	8.87	8.60	11.21	0.82	0.79	0.96
Mean	6.14	6.77	6.54	0.89	0.88	0.97
Sd	1.80	2.06	2.25	0.04	0.16	0.19
R				0.99	0.80	0.80

If the results of the geochemical analyses are compared with the estimates made by GRS (Table 5 and Figure 3), the average values are very similar, being 6.77 μW m^{-3} (standard deviation of 2.06) in the measurements without the collimator and 6.81 μW m^{-3} in those performed with the collimator (standard deviation of 3.20). This indicates that, on average, the estimates made with GRS with a collimator allow an average estimate of RHP to be obtained (Table 5). Comparing the values for each surface, it can be observed that the estimates with the GRS measurements (with and without the collimator) provide a linear correlation coefficient R = 0.99 and an average ratio of 0.89. This implies that regardless of whether or not the collimator is used, the result is very similar. When the measurements obtained without a collimator are compared with the results of the geochemical analyses, excluding samples P7 and P15 (which provide very different results for the three radioisotopes), the coincidence of the results is lower, although the ratio is high, at 0.88 without the collimator and 0.97 with the collimator, and with the linear correlation coefficient being R = 0.80 with and without the collimator. This indicates that GRS is a good tool to estimate RHP, providing a mean deviation of 10% without a collimator and 3% with a collimator.

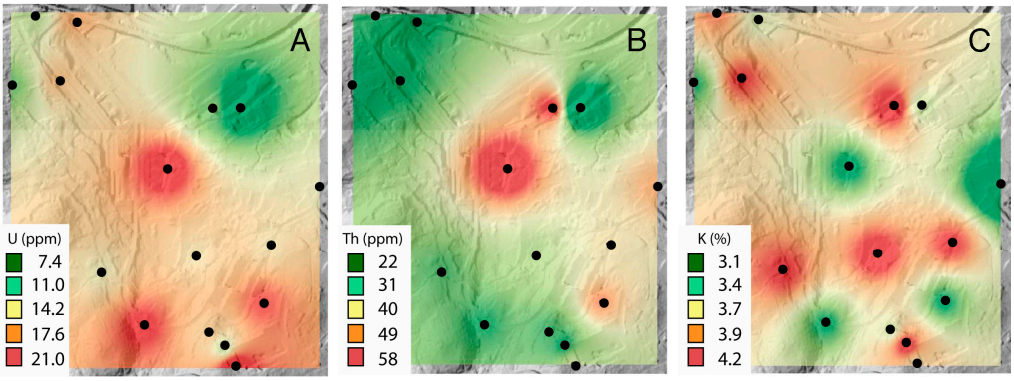

Figure 3. Interpolation map obtained from the GIS with contents of (**A**) U, (**B**) Th, and (**C**) K estimated by geochemical analyses (XRF + ICP-MS).

4.3. Geothermal Potential Map

Using the GIS, maps of the concentrations of U, Th, and K in the subsoil rock were constructed for the area studied. The maps for each chemical element were constructed by interpolation and provide an average estimate of their concentrations in each area of the campus (Figure 3). From these data, a map of the campus was obtained based on the estimates made on the surface. This map allows us to consider the areas with the highest RHP and their situation with respect to the campus buildings. It can also be seen how U is the element that contributes the most to the RHP (Figure 4). Given the high values of U in the rocks studied, the RHP obtained was very high throughout the campus.

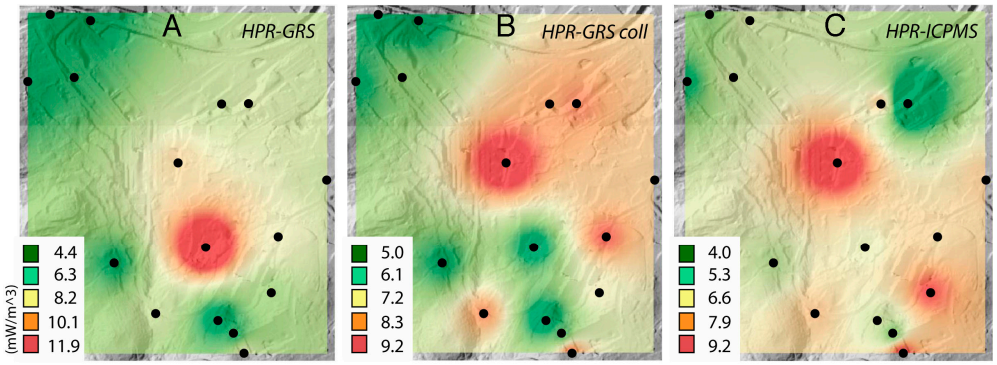

Figure 4. Interpolation maps obtained from the GIS with estimates of radiogenic heat production (RHP) obtained by (**A**) GRS, (**B**) GRS with a collimator, and (**C**) geochemical analyses (XRF + ICP-MS).

Finally, a comparison was made between the RHP map obtained from the geochemical analyses (Figure 4) and the RHP obtained from the estimates made by GRS. The comparison between maps allowed us to verify that the results obtained were very similar. Although the results obtained by GRS with a collimator slightly overestimate those obtained without a collimator, both types of measurements overestimate the data obtained by geochemical analyses on average.

5. Discussion

5.1. Geochemical Analyses

As mentioned in the previous section, the XRF results (Table 2) indicate that the samples fall in the typical range between granodiorites and granites [36], given their SiO_2 and Al_2O_3 contents. The density of the samples also fits with the average values of granodiorites and granites, within the 0.25 percentile [19].

However, the geochemical analyses indicate atypically high concentrations of U, since the expected concentration of U in granodiorites is between 2.2 and 6.1 ppm [27], although the most complete recent study established an average of 3.93 ± 3.27 ppm [18]. In all samples, the concentration of U was above this range, except in the case of sample P7 (2.35 ppm), which showed an atypically low value compared to the rest of the samples. In the case of Th, the values obtained were also higher than expected, since the Th content in granodiorites normally ranges between 8 and 33 ppm [27], although Boyle [38] indicated that it may be higher in granites. Recent studies place its average concentration at 14.8 ± 13.2 ppm [18]. These data allow us to compare the concentration of U with that of Th through the Th/U ratio (Table 4). This ratio is estimated to average 3.7–4.0 in the Earth's crust [39], which implies 3–6 times more Th than U. In the samples studied, the ratio ranged between 0.25 and 0.74 from the geochemical analyses (Table 4), with the average Th/U being 0.49. These values are far from those expected on average for granodiorites and granites, which range between 1 [39] and 3.5–6.3 [27]. Similar values of U and Th have been previously observed in granites from the northwest of the Iberian Peninsula [40]. Therefore, in most samples and for the granodiorites studied, the Th/U ratio was anomalously low [18]. The cause of this anomalous relationship and the abnormally high values of U

and Th is the composition of the rock, since other processes—such as weathering or radon losses—tend to decrease the concentration of U and, therefore, increase the Th/U ratio. This also implies that weathering had not reduced the U concentration, as observed in the most weathered sample (P16), where the Th/U ratio was 0.34 and the U concentration was 24 ppm. Recent studies [13,40] have attributed this high concentration of U to the presence of accessory minerals that contain these elements (i.e., monazite, thorianite, thorite) in granitoids of the area. Similar and anomalously low Th/U ratios have been observed in some Proterozoic granitoids in other areas of the world and, to a lesser extent, in some Palaeozoic ones [18,41].

For K, the results indicate values more in line with those expected in granodiorites and granites [27,39,42], although they are also slightly higher than the average values compiled by Armetieva et al. [18], which were situated at 2.79 ± 1.44%. The average K/U ratio for the Earth's crust has been estimated to be 1.0×10^{-4} [38]. However, in the rocks studied, this ratio was 4.56×10^{-4} for geochemical analyses, 2.60×10^{-4} for those carried out via GRS without a collimator, and 3.41×10^{-4} for those carried out with a collimator (Table 4). These anomalously high ratios have also been observed in some Proterozoic granitoids and, to a lesser extent, in some Palaeozoic ones [18].

In general, the data obtained by GRS—both with and without the use of a collimator—were consistent with the geochemical analyses, with slight differences indicating a tendency to underestimate the concentration of U and to overestimate that of K. Previously, estimates of U, Th, and K have been obtained by GRS in magmatic rocks, in which it has been observed that the GRS tends to overestimate the total gamma radiation [43], although it allows differentiation between rock types in contact zones or zones of heterogeneity, as occurred in the present case study [44].

There are two possible causes for these differences in K and U regarding the estimates obtained by GRS versus geochemical analyses. On the one hand, the peaks used to estimate U and K are ^{214}Bi and ^{40}K, respectively. These peaks have energy values of 1.76 and 1.46 MeV, respectively, making them very similar [28]. This causes one of the two elements to be overestimated when the peak of the other is high. On the other hand, in the measurements made by GRS—and particularly those without a collimator—the geometric effects of the terrain are especially important, so the gamma radiation in the environment can cause the overestimation or underestimation of the radiation rate and the concentrations of U, Th, and K [29]. This was considered and almost all measurements were made using two geometries to avoid these effects, except for surfaces P6, P10, P15, and P16, where this was not possible.

5.2. Geothermal Potential

As mentioned in the Results section, the data obtained indicate a high RHP—greater than 4 μW m^{-3} (Table 5), which can be considered to be a potential indicator of great heat generation and, potentially, an economic source of heat production [29]. The only exception is sample P7 (1.25 μW m^{-3}). This implies that GRS can be considered as a suitable tool to estimate the RHP, providing a mean deviation of 10% without a collimator and 3% with a collimator. It is necessary to consider that the greatest contribution to the surface heat flux varies between 30% and 90% [18], assuming a heat loss of between 30% and 40% in the continental crust [2,18,19].

The comparison between the maps obtained by interpolation indicates the similarity between results with the different analysis methods (Figures 3 and 4). The results obtained indicate a high RHP that can probably be extrapolated to most of the main peraluminous granitoids of northwest Spain and northern Portugal [20,40], although it is necessary to carry out geochemical studies or GRS in other types of granite in this region, given the important regional variability that usually exists in RHP [18]. This high potential was already intuited by Hall et al. [41] and is generalised in Variscan granites (Palaeozoic) due to their geochemistry. However, some recent data compilations indicate that, within the Palaeozoic granites, the studied rock has especially high concentrations of U, along

with above-average concentrations of Th and K [18,19], which means that the RHP is also much higher than the average in Palaeozoic granites (and granites in general). Specifically, according to the data obtained in the study carried out by Hasterok and Webb, this granite would be in the highest 95th percentile among the World's granites in terms of RHP [19].

6. Conclusions

In this work, a geochemical and RHP study of the substrate rock of the main campus of the University of A Coruña was carried out through geochemical analyses and the use of GRS. This study showed the following:

(1) The geochemical analyses of the subsoil rock of the campus indicated that the contents of U, Th, and K are very high—above the expected range for granodiorites and peraluminous granites. The values obtained seemed to fluctuate slightly, and to a greater extent in some areas, due to the heterogeneity of the rock and, partially, to its weathering. In areas of greater weathering, there seemed to be enrichment in U and Th, along with a slight depletion in K.

(2) The comparison of geochemical analyses of U, Th, and K with the data obtained by GRS, both with and without a collimator, showed a good correlation—especially for Th—albeit there was some overestimation. The worst correlation was observed for K.

(3) The RHP values obtained from the geochemical and GRS data were very similar and high at almost all of the sampling points. This indicates that GRS is a fast, inexpensive, and accurate tool for the study of RHP in rocks using data taken from the surface. There was some overestimation; hence, further studies are required, with the aim of establishing some safety criteria, but these results are promising from the perspective of GRS as an exploration tool for delineating the more interesting target areas.

(4) From the geochemical data, the average RHP obtained was 6.54 $\mu W\ m^{-3}$ ($\pm$2.06 $\mu W\ m^{-3}$). This implies a high RHP in almost the entire campus; therefore, this is an energy resource whose exploitation would be profitable to obtain usable heat for heating systems and sanitary running water in the campus buildings.

(5) The granitoids studied in this work extend over almost the entire city of A Coruña and constitute an abundant type of rock in northwest Spain and northern Portugal, indicating that the RHP is probably high in this area and should be studied in detail for the use of geothermal energy in this territory.

Author Contributions: Conceptualisation, J.S.-S. and V.B.R. methodology, J.S.-S. and V.B.R.; software, C.A.C.; validation, J.S.-S., V.B.R. and C.A.; formal analyses and investigation, J.S.-S. and V.B.R.; resources J.S.-S. and V.B.R.; writing—original draft preparation, J.S.-S.; writing—review and editing, C.A.C., V.B.R. and C.A. All authors have read and agreed to the published version of the manuscript.

Funding: This research has been funded by the Consellería de Cultura, Educacion, e Ordenacion Universitaria, Xunta de Galicia, Spain (programmes ED431B 2018/47 and ED431B 2021/17).

Conflicts of Interest: The authors declare no conflict of interest.

References

1. Vitorello, I.; Pollack, H. On the variation of continental heat flow with age and the thermal evolution of the continents. *J. Geophys. Res.* **1980**, *85*, 983–995. [CrossRef]
2. Pollack, H.; Chapman, D. Mantle heat flow. *Earth Planet Sci. Lett.* **1977**, *34*, 174–184. [CrossRef]
3. Cloetingh, S.; Van Wees, J.D.; Ziegler, P.A.; Lenkey, L.; Beekman, F.; Tesauro, M.; Worum, G. Lithosphere tectonics and thermo-mechanical properties: An integrated modelling approach for enhanced geothermal systems exploration in Europe. *Earth Sci. Rev.* **2010**, *102*, 159–206. [CrossRef]
4. Hählein, S.; Bayer, P.; Ferguson, G.; Blum, P. Sustainability and policy for the thermal use of shallow geothermal energy. *Energy Policy* **2013**, *59*, 914–925. [CrossRef]
5. Hébert, R.L.; Ledésert, B.; Bartier, D.; Dezayes, C.; Genter, A.; Grall, C. The enhanced geothermal system of Soultz-Sous-Forêts: A study of the relationships between fracture zones and calcite content. *J. Volcanol. Geotherm. Res.* **2010**, *196*, 126e33. [CrossRef]

6. EU Directive 2009/28/EC of the European Parliament and the Council of 23 April 2009 on the Promotion of the Use of Energy from Renewable Sources and Amending and Subsequently Repealing Directives 2001/77/EC and 2003/30/EC. Available online: https://eur-lex.europa.eu/legal-content/EN/ALL/?uri=celex%3A32009L0028 (accessed on 6 January 2022).
7. IDEA. Evaluación del potencial de energía geotérmica. In *Estudio Técnico PER 2011–2020*; Instituto para la Diversificación y Ahorro de Energía: Madrid, Spain, 2011.
8. Chamorro, C.R.; García-Cuesta, J.L.; Mondéjara, M.E.; Linares, M.M. An estimation of the enhanced geothermal systems potential for the Iberian Peninsula. *Renew. Energy* **2014**, *66*, 1–14. [CrossRef]
9. EGEC. The geothermal energy market grows exponentially, but needs the right market conditions to thrive. In *EGEC Releases the European Geothermal Market Report 2019*; European Geothermal Energy Council: Brussels, Belgium, 2020. Available online: https://www.egec.org/the-geothermal-energy-market-grows-exponentially-but-needs-the-right-market-conditions-to-thrive/ (accessed on 6 January 2020).
10. EGEC. Renewables—Global Status Report REN21. Renewable Energy Policy Network for the 21st Century. European Geothermal Energy Council, 2009. Available online: https://www.unep.org/resources/report/renewables-2021-global-status-report (accessed on 2 November 2022).
11. IGME. *Inventario General de Manifestaciones Geotérmicas en el Territorio Nacional. Plan Nacional de Minería*; Ministerio de Industria: Tokyo, Japan, 1975.
12. VDI 4640 Blatt 2: 2001-09 Thermische Nutzung des Untergrundes; Erdgekoppelte Wärmepumpenanlagen (Thermal Use of the Underground Ground Source Heat Pump Systems). Verein Deutscheringenieure. Available online: https://www.beuth.de/de/technische-regel/vdi-4640-blatt-2/43607817 (accessed on 6 August 2020).
13. Sanjurjo-Sánchez, J.; Barrientos Rodríguez, V. Reevaluación del potencial geotérmico de los granitos de Galicia en base a cartografía geoquímica y radiológica. *Cad. Lab. Xeolóxico Laxe* **2018**, *40*, 123–138. [CrossRef]
14. MARNA. *Mapa de Radiación Gamma de España. Escala 1:1.000.000*; Consejo de Seguridad Nuclear: Madrid, Spain, 2001.
15. Consejo de Seguridad Nuclear. *Cartografía de Potencial de Radón de España. Escala 1:200.000*; Consejo de Seguridad Nuclear: Madrid, Spain, 2017.
16. IGME. *Atlas Geoquímico de España*; Instituto Geológico y Minero de España: Madrid, Spain, 2012.
17. Vilà, M.; Fernández, M.; Jiménez-Munt, I. Radiogenic heat production variability of some common lithological groups and its significance to lithospheric thermal modeling. *Tectonophysics* **2010**, *490*, 152–164. [CrossRef]
18. Artemieva, I.M.; Thybo, H.; Jakobsen, K.; Sørensen, N.K.; Nielsen, L.S.K. Heat production in granitic rocks: Global analysis based on a new data compilation GRANITE2017. *Earth-Sci. Rev.* **2017**, *172*, 1–26. [CrossRef]
19. Hasterok, D.; Webb, J. On the radiogenic heat production of igneous rocks. *Geosci. Front.* **2017**, *8*, 919–940. [CrossRef]
20. Cuesta, A.; Gallastegui, G. Magmatismo de la Zona Centroibérica: Galicia occidental. In *Geología de España*; Vera, J.A., Ed.; SGE-IGME: Madrid, Spain, 2004; pp. 96–100.
21. Cermak., V.; Huckenholz, H.G.; Rybach, L.; Shmid, R.; Schopper, J.R.; Schuch, M.; Stöffler, D.; Wohlenberg, J. Thermal properties: Thermal conductivity and specific heat of minerals and rocks. In *Landolt-Brnstein Zahlenwerte und funktionen aus Naturwissenschaften und Technik. Neue Serie, Physikalische Eigenschaften der Gesteine*; Angeneister, G., Ed.; Spriger: Berlin/Heidelberg, Germany; New York, NY, USA, 1982; pp. 305–343.
22. Rybach, L. Determination of heat production rate. In *Handbook of Terrestrial Heat Flow Determination*; Rybach, R., Rybach, L., Stegena, L., Eds.; Kluwer: Dordrecht, The Netherlands, 1988; pp. 125–142.
23. Rybach, L. *Radioactive Heat Production: A Physical Property Determined by the Chemistry in the Physical and Chemistry of Minerals and Rocks*; Strens, R.G.J., Ed.; A Wiley-Interscience Publication: New York, NY, USA, 1976.
24. Ashwal, L.; Morgan, P.; Kelley, S.; Percival, J. Heat production in an Archean crustal profile and implications for heat flow and mobilization of heat-producing elements. *Earth Planet Sci. Lett.* **1987**, *85*, 439–450. [CrossRef]
25. Singh, A.K.; Vallinayagam, G. Geochemistry and petrogenesis of anorogenic basic volcanic-plutonic rocks of the Kundal area of Malani Igneous Suite, Western Rajasthan, India. *Proc. Ind. Acad. Sci. (Earth Planet. Sci.)* **2004**, *113*, 667–681. [CrossRef]
26. Darnley, A. *A Global Geochemical Database for Environmental and Resource Management*; UNESCO Publishing: Ottawa, SO, Canada, 1995; p. 122.
27. Gascoyne, M. Geochemistry of the actinides and their daughters. In *Uranium-Series Disequilibrium: Applications to Earth, Marine, and Environmental Sciences*; Ivanovich, M., Harmon, R.S., Eds.; Clarendon Press: Oxford, UK, 1992; pp. 34–61.
28. Erdi-Krausz, G.; Matolin, M.; Minty, B.; Nicolet, J.; Reford, W.; Schetselaar, E. *Guidelines for Radioelement Mapping Using Gamma Ray Spectrometry Data*; International Atomic Energy Agency: Vienna, Austria, 2003.
29. McCay, A.T.; Harley, T.L.; Younger, P.L.; Sanderson, D.C.W.; Cresswell, A.J. Gamma-ray spectrometry in geothermal exploration: State of the art techniques. *Energies* **2014**, *7*, 4757–4780. [CrossRef]
30. Castro, A.; Corretgé, L.G.; De la Rosa, J.; Enrique, P.; Martínez, F.J.; Pascual, E.; Lago, M.; Arranz, E.; Galé, C.; Fernández, C.; et al. Palaeozoic Magmatism. In *The Geology of Spain*; Gibbons, W., Moreno, T., Eds.; Geological Society of London: London, UK, 2022; pp. 117–153.
31. Bellido Mulas, F.; González Lodeiro, F.; Klein, E.; Martínez Catalán, J.R.; Pablo Macía, J.G. *Las rocas graníticas hercínicas del norte de Galicia y occidente de Asturias. Memorias Instituto Geológico y Minero de España, t. 101*; IGME: Madrid, Spain, 1987; 157p.
32. Cuesta, A. Petrología granítica del plutón de Caldas de Reyes (Pontevedra, España) Estructura, mineralogía, química y petrogénesis. *Nova Terra O Castro* **1991**, *5*, 363.

33. IGME. *Mapa Geológico de España 1:50.000 MAGNA*; Instituto Geológico y Minero de España: Madrid, Spain, 2015. Available online: https://igme.maps.arcgis.com/home/webmap/viewer.html?webmap=92d3a8e400b44daf911907d3d7c8c7e9 (accessed on 15 October 2022).
34. Agencia de Ecología Urbana de Barcelona, Diagnose Enerxética, Campus de Elviña e da Zapateira, Universidade da Coruña, 2010
35. cnig-IGN. MDT05-LiDAR Digital Terrain Models, Sh eets H0021 and H0045. In *Centro Nacional de Información Geográfica*; Instituto Geográfico Nacional: Madrid, Spain, 2009; Available online: https://centrodedescargas.cnig.es/CentroDescargas/index.jsp (accessed on 15 October 2022).
36. Best, M.G.; Christiansen, E.H. *Igneous Petrology*; Blackwell Science: Oxford, UK, 2001; 458p.
37. Irfan, T.Y.; Dearman, W.R. Engineering classification and index properties of a weathered granite. *Bull. Int. Assoc. Eng. Geol.* **1978**, *17*, 79–90. [CrossRef]
38. Boyle, R.W. *Geochemical Propecting for Thorium and Uranium Deposits*; Elsevier: New York, NY, USA, 1982; 489p.
39. Taylor, S.R.; McLennan, S.M. *The Continental Crust: Its Composition and Evolution*; Blackwell Scientific Publications: Hoboken, NJ, USA, 1985; p. 312.
40. Lima, M.; Alves, C.; Sanjurjo-Sanchez, J. Gamma radiation in rocks used as building materials: The braga granite (Nw Portugal). *Cad. Lab. Xeolóxico Laxe* **2015**, *38*, 81–93. [CrossRef]
41. Hall, A. *Igneous Petrology*, 2nd ed.; Longman Limited: Essex, UK, 1996; 551p.
42. Clarke, D.B. *Granitoid Rocks*, 1st ed.; Chapman & Hall: London, UK, 1992.
43. Couto, M.; Sanjurjo-Sanchez, J.; Alves, C. Advances in Materials Science and Engineering Assessment of Gamma Radiation Hazards Related to Geologic Materials: Comparison of Results by Field Gamma Spectrometry and Laboratory Methods. *Adv. Mater. Scid. Eng.* **2018**, *13*, 1–9. [CrossRef]
44. Dias, F.; Lima, M.; Sanjurjo-Sanchez, J.; Alves, C. Analysis of spectra from portable handheld gamma-ray spectrometry for terrain comparative assessment. *J. Environ. Radioact* **2016**, *154*, 93–100. [CrossRef] [PubMed]